

Laser writing of scalable single colour centre in silicon carbide

Yu-Chen Chen^{1*}, Patrick S. Salter², Matthias Niethammer¹, Matthias Widmann¹, Florian Kaiser¹, Roland Nagy¹, Naoya Morioka¹, Charles Babin¹, Jürgen Erlekamp³, Patrick Berwian³, Martin Booth², Jörg Wrachtrup¹

1. 3rd Institute of Physics, University of Stuttgart and Institute for Quantum Science and Technology IQST, Germany
2. Department of Engineering Science, University of Oxford, Parks Road, Oxford OX1 3PJ, UK
3. Fraunhofer IISB, D-91058 Erlangen, Germany

*Corresponding author: y.chen@pi3.uni-stuttgart.de

Abstract:

Single photon emitters in silicon carbide (SiC) are attracting attention as quantum photonic systems [1-2]. However, to achieve scalable devices it is essential to generate single photon emitters at desired locations on demand. Here we report the controlled creation of single silicon vacancy (V_{Si}) centres in 4H-SiC using laser writing without any post-annealing process. Due to the aberration correction in the writing apparatus and the non-annealing process, we generate single V_{Si} centres with yields up to 30%, located within about 80 nm of the desired position in the transverse plane. We also investigated the photophysics of the laser writing V_{Si} centres and conclude that there are about 16 photons involved in the laser writing V_{Si} centres process. Our results represent a powerful tool in fabrication of single V_{Si} centres in SiC for quantum technologies and provide further insights into laser writing defects in dielectric materials.

Introduction

Silicon carbide (SiC) is host to many promising colour centres with extremely high brightness [3-7] and long spin coherence time [8-11], showing favourable properties as quantum light sources and providing optical interfaces with electron and nuclear spins. In particular, silicon vacancy (V_{Si}) defects in SiC have shown to be useful for high-precision vector magnetometry [12,13], all-optical magnetometry [14], thermometry [15] and quantum photonics [16,17].

To provide scalable quantum technologies based on V_{Si} centres in SiC, it will be necessary to integrate those systems into nanophotonics and electronics functional structures [8,16,17] with an accuracy of 10 nm - 1 μ m. In this regard, focused Si ion and proton beams have been used to engineer V_{Si} centres in SiC with high spatial accuracy [18,19]. However, those methods come at the expense of creating considerable residual lattice damage, which may reduce spin and optical coherence properties. Recently, the laser writing method was successfully implemented to generate single nitrogen vacancy centres in diamond with high positioning accuracy and near-unity yield, while maintaining excellent spin and optical coherence properties [20-22]. Moreover, laser writing method has recently successfully generated V_{Si} centres ensembles in 4H-SiC at various depth [23].

In this work, we apply the laser writing method to fabricate single V_{Si} centres in 4H polytype of SiC with high yield and good optical properties. Due to the combination of nonlinear laser writing process and appropriate aberration correction [20, 21], our method can generate defects at any depth in the crystal and with a spatial resolution beyond the optical diffraction limit. We also discuss the mechanism of the laser writing process.

Main text

Our host material is a 4H-SiC epitaxial layer that was grown along c-axis in an Epigress CVD reactor (VP508) at 1625 °C with nitrogen doping of $1 \times 10^{15} \text{ cm}^{-3}$ and the a thickness of $62 \mu\text{m}$ on an 4° off-axis 4H-SiC substrate. Then, the sample was oxidized in oxygen atmosphere at 1300 °C for 5.5 hours and subsequently annealed in Argon atmosphere at 1500 °C to minimize the carbon vacancy (V_c) concentration.

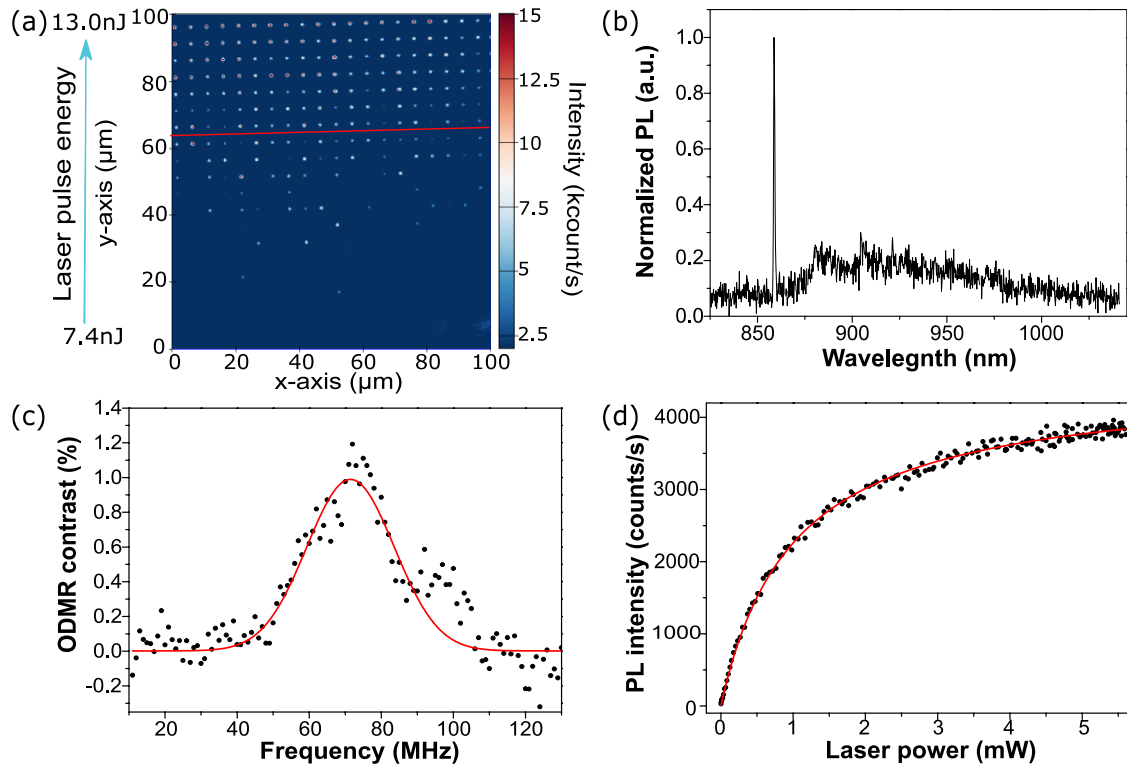


Figure 1. Generation of V_{Si} centres using laser writing. (a) PL image of Array A immediately after laser processing. The laser pulse energy increases from the bottom to the top of the image and the range of the laser pulse energy used are provided on the left of the figure. The red line at the pulse energy of 12.6 nJ indicates the pulse energy threshold to generate colour centres in all 20 repeats. (b) Typical spectrum at 4.2 K of the features generated with laser pulse energy lower than 12.6 nJ, which indicates the generation of hexagonal lattice site V_{Si} centres ($V1'$). (c) Typical ODMR signal of the laser written V_{Si} centres ensemble at room temperature, revealing cubic lattice site V_{Si} centres ($V2$). (d) Typical background-corrected excitation power dependent fluorescence of laser written single V_{Si} centre. The linearly increasing background fluorescence was recorded by when being aligned for away from the emitter.

We characterized the sample via photoluminescence (PL) detection using a confocal microscope arrangement (see Supporting information). Our initial PL scans of the sample allowed us to identify large regions without 'native' V_{Si} centres, which were subsequently chosen to conduct the laser writing experiments. Single writing pulses of wavelength 790 nm and duration 250 fs were delivered to each site in 40×20 square grids with a pitch of $5 \mu\text{m}$ at a depth of $20 \mu\text{m}$. Along the vertical axis of the grids, the pulse energy, E_p , was varied from 6.7 nJ to 89.4 nJ to generate incremental degrees of damage to the lattice (see Supporting Information for more details). Along the horizontal axis, 20 identical pulses were delivered to perform statistics for each pulse energy. In this paper, this array is labelled as Array A. Additionally, we also generated a second array at a deeper depth of $40 \mu\text{m}$ with

single writing pulses for each site to demonstrate the 3D ability of laser writing (see Figure S2 in Supporting Information). This deeper array will be called Array B.

Figure 1a shows a PL image of Array A immediately after laser writing without annealing or other treatments. Since the size of Array A is much larger than the scan range of our confocal microscope, we only show the PL image of the area exposed to the laser pulse energy from 7.4 to 15.6 nJ in Figure 1a (from bottom to top). At a threshold pulse energy of $E_p \geq 12.6$ nJ fluorescence was observed at each site (red line in Figure 1a). As E_p decreases from 12.6 nJ, the probability for defect generation among 20 repeats drops. Furthermore, no visible fluorescent sites are observed for $E_p \leq 8.2$ nJ. These findings indicate that the average number of colour centres' per site decrease as a function of laser pulse energy.

Figure 1b shows the typical emission spectrum of a laser written feature at 4.2 K. The spectrum shows a sharp peak at 858.7 nm with roughly 100 nm wide phonon side band, which corroborates the generation of hexagonal lattice site silicon carbide centres [24]. Note that the sharp peak at 858.7 nm corresponds to the optical transition between the ground state and the second excited state V1' of the V_{Si} centre [25]. Since in our optical arrangement, we collect fluorescence almost parallel to the c-axis of 4H-SiC, we cannot observe emission from the first excited state V1, whose dipole orientation is parallel to the c-axis [24,25]. For the same reason, we do also not observe emission from cubic lattice site V_{Si} centres (V2). They are even not seen in the spectrum of the heavy damage alignment markers (see Supporting Information), as shown in Figure S4 in the Supporting Information. At sites fabricated with high laser pulse energy, there may be many V2 V_{Si} centres generated, but their emission is weak and covered by the V1' emission. However, due to the different zero-field splitting energies of V1 and V2 V_{Si} centres, the optically detected magnetic resonance (ODMR) measurements can distinguish the emission of V2 from V1 V_{Si} centres. The ODMR measurements were performed on the laser written V_{Si} centres ensemble at room temperature. 6 out of 10 sites written with $E_p \geq 22.7$ nJ show a clear ODMR signal at around 70 MHz at zero external field indicating the existence of V2 V_{Si} centres by its characteristic zero field splitting, as shown in Figure 1c. The red line is the best fit to a Gaussian function, giving the peak position at 71.5 ± 0.41 MHz. The observed side peaks are due to a small inhomogeneous parasitic magnetic field from the experimental apparatus [13].

Figure 1d shows the excitation power dependent fluorescence intensity for a single hexagonal site V_{Si} centre at room temperature. The intensity $I(P)$ can be described by the formula

$$I(P) = \frac{PI_{sat}}{P + P_{sat}}, \quad (1)$$

where I_{sat} is the saturation intensity and P_{sat} is the saturation power of the emitter. The red line in Figure 1d is the best fit to Equation (1), giving $I_{sat} = 4526 \pm 17$ counts/s and $P_{sat} = 1.00 \pm 0.02$ mW. Note that I_{sat} is 2 to 3 times lower than previously reported values, which is due to the deep location of the laser written V_{Si} centres [8, 19, 26]. We expect similar PL intensity when the defects are created more shallow (few μm below surface).

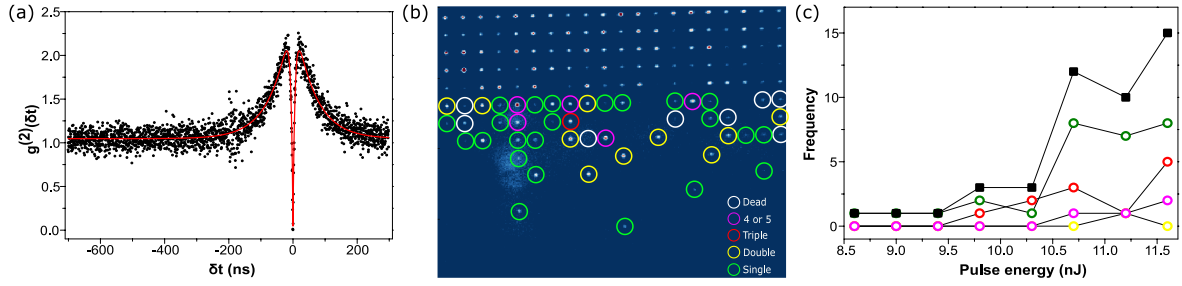


Figure 2. Statistics of V_{Si} centres generation using laser processing. (a) Typical $g^{(2)}(\delta t)$ histogram from single V_{Si} centre after background removal at room temperature. (b) Map of the number of V_{Si} centres generating at different sites in Array A. ‘Dead’ refers to the centres which photobleached during $g^{(2)}(\delta t)$ measurements. (c) Plot of the number of single (green), double (yellow), triple (red), and 4 or 5 (purple) V_{Si} centres generated in each row of 20 repeats as a function of laser pulse energy measured before the objective lens in the writing apparatus. The total number generated per row is presented in black.

Photon autocorrelation measurements (see Methods) were conducted for each site with $E_p \leq 11.6$ nJ in Array A to determine the number of V_{Si} centres. Since the detected PL count rate is low (4–14 kcounts/s), the background fluorescence (about 1.0 kcounts/s) needs to be accounted for in the second order autocorrelation histogram $g^{(2)}(\delta t)$ (see Method for detail). Fig 2a shows a typical data set displaying a distinct photon anti-bunching at $\delta t = 0$ with $g^{(2)}(\delta t) = 0.040 \pm 0.003$, which stands as a clear characteristic of a single colour centre. In addition, for $|\delta t| > 16.5$ ns we observe a significant bunching behaviour, which is typical for a three-level like the one investigated here (see Method).

Figure 2b shows a spatial map of the V_{Si} populations per laser writing site of Array A. In spots that have been created using lower pulse energies, all V_{Si} centres are optically stable. At sites $E_p > 10.7$ nJ, 2 to 3 laser written V_{Si} centres among 20 repeats were photobleached after a few hours optical excitation and 1 to 2 V_{Si} centres showed blinking behaviour. Combining these observations, we suggest that the optical instability may be attributed to the charge transfer from the V_{Si} centres to other laser generated defects in the vicinity, such as carbon vacancies (V_C), C interstitial and Si interstitial defects. To our best knowledge, these phenomena were not observed in V_{Si} centres generated by electron irradiation. A likely explanation is that, in laser writing, there is a higher chance of creating the V_C centres, C interstitial and Si interstitial defects in the vicinity of the V_{Si} centres, as the laser energy is focused into a small volume around the position where the V_{Si} centre is generated. Oshima et al proposed that the post irradiation annealing may be able to remove unwanted defects and stabilize the V_{Si} centres [27]. The optical stability of laser written V_{Si} centres may be improved by adjusting the n-doping level [28]. Although some V_{Si} centres are not optically stable, at 10.7 nJ, 6 out of 20 sites revealed an optically stable single V_{Si} , corresponding to a probability of 30%. Figure 2c shows the statistics of each row in Array A as a function of the laser writing pulse energy. Here, the number of V_{Si} centres in photobleached sites is estimated from the initial PL count rate. The total number of V_{Si} centres generated per row shows a systematic increase with the laser pulse energy. The probability of fabricating single V_{Si} centres also increases with writing pulse energy and reaches its maximum at after a pulse energy of 10.7 nJ. The number of multiple V_{Si} centres per row increase with pulse energy, as well.

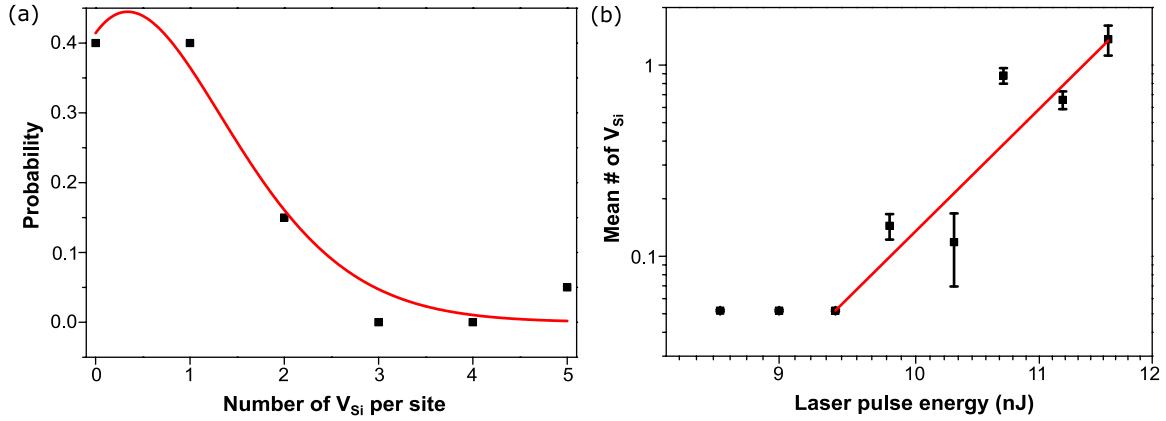


Figure 3. Nonlinearity of the laser writing process. (a) Statistical distribution of the number of the V_{Si} centres per laser writing site at laser pulse energy of 10.7 nJ. The probability value is the ratio between the number of site for each case of number of V_{Si} per site and 20 repeats. (b) The average number of the V_{Si} centres per laser writing site among 20 repeats as a function of laser pulse energy.

In the following, we discuss the mechanism of laser writing of the V_{Si} centres in SiC. First, we consider the statistics of the distribution of the population of V_{Si} centres per site for 20 repeats for each writing pulse energy. Figure 3(a) shows the results of sites written with a pulse energy of 10.7 nJ, as an example. The red line in Figure 3(a) is a least-squares fit of the Poisson distribution function, $P_{\lambda}(k) = \frac{\lambda^k e^{-\lambda}}{k!}$. Here λ is the average number of V_{Si} centres per site and k is the number of V_{Si} centres generated per site. At writing pulse energy of 10.7 nJ, the Poisson distribution fit gives $\lambda = 0.88 \pm 0.08$. The mean value for generated V_{Si} from the Poisson fits is plotted in Figure 3b as a function of writing pulse energy with the error bars representing the fitting error. Note that any laser generated V_{Si} centres which may have been present but in the wrong charge state at the beginning or were photobleached during PL scan are not taken into account. Thus, our data analysis represents a lower limit case. In the region between 8.6 and 9.4 nJ, the average number of generated V_{Si} centres remains constant, possibly because there are not enough repeats to sufficiently evaluate them statistically. For this reason, we exclude the first two data points in the following analysis. The average number of V_{Si} centres per site exponentially increases with the writing pulse energy at $E_p > 9.4$ nJ, which is similar to laser writing defect generation in diamond [29]. Lagomarsino et al in ref 28 demonstrated that the dominant free electrons generation mechanism at low writing pulse energy is multiphoton ionization (MPI). Thus, we think that the MPI can describe the mechanism of the laser writing V_{Si} centres as the writing pulse energy is lower than 12 nJ (see Supporting Information). The photonization rate of MPI can be expressed as

$$P(E) = \sigma_k E_p^k, \quad (2)$$

where σ_k is the multiphoton absorption coefficient for the absorption of k photons and E_p is the writing pulse energy [30]. The red line in Figure 3b is the least-squares fit of Equation (2), giving $k = 15.5 \pm 1.2$. In other words, each photon in the 790 nm laser pulse possesses an energy of 1.57 eV, implying that energy is transferred to the SiC lattice in packets of 24.33 ± 1.88 eV. The displacement threshold energy for Si atom in SiC is approximately 25 eV [31], which falls within the error bar of our result. Note that the 15.5 photon absorption obtained here is the nonlinearity of vacancy generation instead of the free electron generation in ref 29. To date, it remains still unclear how the free electrons convert to defects for ultrafast laser pulse writing in wide bandgap materials. The

nonlinearity analysis merely provides an insight into certain aspects of the mechanism for defects generation in SiC.

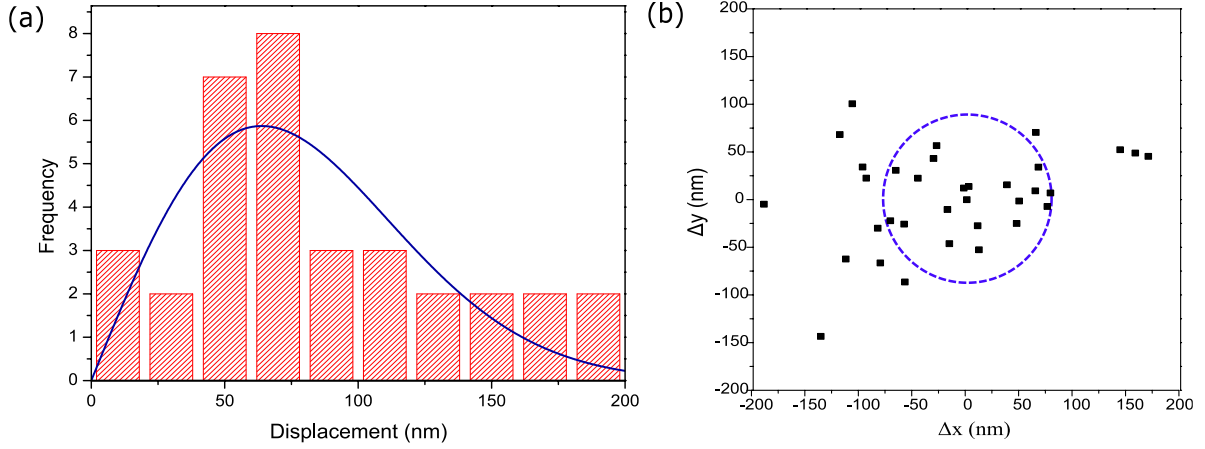


Figure 4. Positioning accuracy of the V_{Si} centres generation using laser processing. (a) Histogram of the displacement in the image plane for the V_{Si} centres. The data are fitted with a Rayleigh distribution function. (b) Scatter plot of the fitted positions of the V_{Si} centres relative to the theoretical grid points in the image plane. The dashed circle represents the mean displacement obtained from fitting in (a).

For applications, it is important that the V_{Si} centres can be accurately positioned in 3D in order to integrate them into other device architectures. The precision with which we can position V_{Si} centres in the image plane was obtained by fitting a 2D Gaussian surface to the measured intensity distribution of each laser written V_{Si} centre. The theoretical grid points were determined by conducting a least-squares fit of a regular square grid with 5 μm grid length to laser written V_{Si} centres' positions using fitting parameters of displacement in x and y. The obtained displacements between the V_{Si} centres and the theoretical grid points are plotted as a histogram in Figure 4a. The blue line is the best fit to a Rayleigh distribution, giving a mean displacement of 80 ± 9 nm. Figure 4b shows the spatial distribution of the V_{Si} centres' positions relative to their theoretical grid points and the dashed circle is the mean displacement. The mean displacement is a factor of 3.7 smaller than the diffraction limited width of the focal spot of the writing laser (see Supporting Information), which underlines the great potential of the laser writing method to precisely generate on-demand defects in photonic structures.

The nonlinearity of the MPI mechanism is expected to result in vacancy creation within a region smaller than the focal volume estimated by the field intensity $I(r, z)$ (Equation S1 in Supporting Information). According to MPI model, the spatial distribution function for vacancy generation via a y-photon absorption process is dependent on $I^y(r, z)$ and the corresponding full width at half maximum (FWHM) in radial and axial directions are given by

$$d_y = \omega_0 \sqrt{\frac{2 \ln 2}{y}}, L_y = 2z_R \sqrt{2^{\frac{1}{y}} - 1}. \quad (3)$$

In the previous section, we have demonstrated that 15.5 photons are involved in the vacancy generation process. As a result, the $d_{15.5}$ and $L_{15.5}$ are corresponding to 88.8 and 364.4 nm,

respectively. The estimated radial FWHM matches well with the measured mean displacement. We note that the positioning accuracy could be better than the estimated radial FWHM. The probability of vacancy creation is related to the writing pulse energy, and there is a threshold energy required before there is a significant probability of vacancy generation. When the writing pulse energy is only slightly above the threshold, the volume with measurable probability of vacancy generation could be smaller than the estimated volume from Equation 3. Chen et al recently demonstrated that the radial positioning accuracy of laser written single NV⁻ centres in diamond is about 40 nm [21], which is half the measured positioning accuracy of V_{Si} centres here. This may be due to a little spherical aberration in our PL image. In addition, many V_{Si} centres created by relatively high writing pulse energy were included in the positioning accuracy analysis in this work.

Summary

In summary, we have demonstrated femtosecond laser writing of single V_{Si} centres into SiC at predefined positions. The yield of optically stable single V_{Si} centres is up to 30%. In diamond, some form of annealing is always required to generate NV⁻ centres [20-22]. On the contrary, single V_{Si} centres in SiC can be created with just a single pulse and no annealing. We note that additional annealing may be used to remove unwanted laser generated defects in order to improve the stability of the V_{Si} centres and further improve the yield. The 80 ± 9 nm positioning accuracy in the image plane was achieved, which is sufficient for coupling V_{Si} centres to optical structures such as multimode waveguides, whispering gallery resonators [32], solid immersion lenses [8], or nanopillars [16]. The positioning accuracy may be limited by the relatively high writing pulse energy range, aberrations of detection apparatus and translational uncertainty of the stage control in the laser writing apparatus. The positioning accuracy of generating V_{Si} centres can be possibly improved down to 40 nm, which has been already demonstrated in diamond [21], providing sufficient resolution to couple to nanophotonic structures [17]. The targeted laser writing V_{Si} centres technique presented here can be applied on SiC with different polytypes, such as 3C and 6H. Since the count rate of V_{Si} centres fluorescence is low, it is necessary to couple the V_{Si} centres to photonic structure to measure the spin coherence time and line width of ZPL. In the future, we will laser write the V_{Si} centres into solid immersion lenses or nanocavities to investigate the spin and optical coherence properties. Also, direct detection during laser writing might be used to allow the on-demand vacancy creation with instant success feedback. In addition, the laser writing method and subsequent annealing may generate other colour centres in SiC, such as divacancy [9,11], carbon antisite-vacancy pairs (V_{Si}V_C)⁰ [6] and nitrogen vacancy (N_CV_{Si})⁻ [33].

Method

Photon autocorrelation measurements and data fitting

Photon autocorrelation datasets were measured using the Hanbury Brown and Twiss method, using continuous wave 730 nm excitation at a power of 1.2 mW. A 850 nm long-pass filter was used for spectrally filtering. Background signals were measured by recording the fluorescence signal from the bulk SiC at a position off-focus from the laser writing site, used to calculate the baseline for the autocorrelation dataset according to the function

$$a = \frac{S}{S + B}$$

where S and B are the photon count rates for the colour centres and the background fluorescence respectively. The background baseline of the raw datasets, $g_{raw}^{(2)}(\delta t)$, is corrected according to the formula

$$g^{(2)}(\delta t) = \frac{g_{raw}^{(2)}(\delta t) - (1 - a^2)}{a^2}$$

The dataset with background correction in Figure 2a were fitted by a standard function for the photon autocorrelation of a three-level system:

$$g^{(2)}(\delta t) = 1 - c \exp\left(\frac{-|\delta t|}{\tau_1}\right) + (c - 1) \exp\left(\frac{-|\delta t|}{\tau_2}\right)$$

where c , τ_1 and τ_2 are related to the interlevel rate constants. The solid red line is a least-squares fit of this equation to the experimental data.

Reference

- [1] Awschalom, D. D.; Hanson, R.; Wrachtrup, J.; & Zhou, B. B. Quantum technologies with optically interfaced solid-state spin. *Nat photon*. 2018, 12, 516-527.
- [2] Atatüre, M.; Englund, D.; Vamivakas, N.; Lee, S. Y.; & Wrachtrup, J. Material platforms for spin-based photonic quantum technologies. *Nat Rev Mater*. 2018, 3, 38-51.
- [3] Castelletto, S.; Johnson, B. C.; Ivady, V.; Stavrias, N.; Umeda, T.; Gali, A.; & Ohshima, T. A. Silicon carbide room-temperature single-photon source. *Nat. Mater*. 2013, 13, 151–156.
- [4] Khramtsov, I. A.; Vyshnevyy, A. A.; & Fedyanin, D. Yu. Enhancing the brightness of electrically driven single-photon sources using color centers in silicon carbide. *Npj Quantum Inf*. 2018, 4, 15.
- [5] Wang, J.; Zhou, Y.; Wang, Z.; Rasmita, A.; Yang, J.; Li, X.; von Bardeleben, H. J.; & Gao, W. Bright room temperature single photon source at telecom range in cubic silicon carbide. *Nat. Commun*. 2018, 9, 4106.
- [6] Lienhard, B.; Schröder, T.; Mouradian, S.; Dolde, F.; Tran, T. T.; Aharonovich, I.; & Englund, D. Bright and photostable single-photon emitter in silicon carbide. *Optica*. 2016, 3, 768-744.
- [7] Widmann, M.; Niethammer, M.; Makino, T.; Rendler, T.; Lasse, S.; Ohshima, T.; Ul Hassan, J.; Son, N. T.; Lee, S. Y.; & Wrachtrup, J. Bright single photon sources in lateral silicon carbide light emitting diodes. *Appl. Phys. Lett*. 2018, 112, 231103.
- [8] Widmann, M.; Lee, S. Y.; Rendler, T.; Son, N. T.; Fedder, H.; Paik, S.; Yang, L. P.; Zhao, N.; Yang, S.; Booker, I.; Denisenko, A.; Jamal, M.; Momenzadeh, S. Al; Gerhardt, I.; Ohshima, T.; Gali, A.; Janzen, E.; & Wrachtrup, J. Coherent control of single spins in silicon carbide at room temperature. *Nat. Mater*. 2014, 14, 164–168.
- [9] Seo, H.; Falk, A. L.; Klimov, P. V.; Miao, K. C.; Galli, G.; & Awschalom, D. D. Quantum decoherence dynamics of divacancy spins in silicon carbide. *Nature Commun*. 2016, 7, 12935.
- [10] Yang, L. P.; Burk, C.; Widmann, M.; Lee, S. Y.; Wrachtrup, J.; & Zhao, N. Electron spin decoherence in silicon carbide nuclear spin bath. *Rev. B: Condens. Matter Mater. Phys*. 2014, 90 (24), 241203.
- [11] Christle, D. J.; Falk, A. L.; Andrich, P.; Klimov, P. V.; Hassan, J. U.; Son, N. T.; Jánzén, E.; Ohshima, T.; & Awschalom, D. D. Isolated electron spin in silicon carbide with millisecond coherence times. *Nat. Mater*. 2014, 14 (2), 160–163.
- [12] Lee, S. Y.; Niethammer, M.; & Wrachtrup, J. Vector magnetometry based on S=3/2 electronic spins. *Phys. Rev. B* 2015, 92, 115201.
- [13] Niethammer, M.; Widmann, M.; Lee, S. Y.; Stenberg, P.; Kordina, O.; Ohshima, T.; Son, N. T.; Jánzén, E.; & Wrachtrup, J. Vector magnetometry using silicon vacancies in 4H-SiC under ambient conditions. *Phys. Rev. Appl*. 2016, 6, 034001.
- [14] Simin, D.; Soltamov, V. A.; Poshakinskiy, A. V.; Anisimov, A. N.; Babunts, R. A.; Tolmachev, D. O.; Mokhov, E. N.; Trupke, M.; Tarasenko, S. A.; Sperlich, A.; Baranov, P. G.; Dyakonov, V.; & Astakhov, G. V. All-optical dc nanotesla magnetometry using silicon vacancy fine structure in isotopically purified silicon carbide. *Phys. Rev. X* 2016, 6, 031014.

- [15] Anisimov, A. N.; Simin, D.; Soltamov, V. A.; Lebedev, S. P.; Baranov, P. G.; Astakhov, G. V.; & Dyakonov, V. Optical thermometry based on level anticrossing in silicon carbide. *Sci. Rep.* 2016, 6, 33301.
- [16] Radulaski, M.; Widmann, M.; Niethammer, M.; Zhang, J. L.; Lee, S. Y.; Rendler, T.; Lagoudakis, K. G.; Son, N. Tien; Janzen, E.; Ohshima, T.; & Wrachtrup, J. Scalable Quantum Photonics with Single Color Centers in Silicon Carbide. *Nano Lett.* 2016, 1612, 02874.
- [17] Bracher, D. O.; Zhang, X. Y.; & Hu, E. L. Selective Purcell enhancement of two closely linked zero-phonon transitions of a silicon carbide color center. *Proc. Natl. Acad. Sci. U. S. A.* 2016, 1609, 03918.
- [18] Kraus, H.; Simin, D.; Kasper, C.; Suda, Y.; Kawabata, S.; Kada, W.; Honda, T.; Hijikata, Y.; Ohshima, T.; Dyakonov, V.; & Astakhov, G. V. Three-dimensional proton beam writing of optically active coherent vacancy spins in silicon carbide. *Nano Lett.* 2017, 17, 2865.
- [19] Wang, J.; Zhang, X.; Zhou, Y.; Li, K.; Wang, Z.; Peddibhotla, P.; Liu, F.; Bauerdick, S.; Rudzinski, A.; Liu, Z.; & Gao, W. Scalable fabrication of single silicon vacancy defect arrays in silicon carbide using focused ion beam. *ACS Photonics.* 2017, 4, 1054.
- [20] Chen, Y.-C.; Salter, P. S.; Knauer, S.; Weng, L.; Frangeskou, A. C.; Stephen, C. J.; Ishmael, S. N.; Dolan, P. R.; Johnson, S.; Green, B. L.; Morley, G. W.; Newton, M. E.; Rarity, J. G.; Booth M. J.; & Smith, J. M. Laser writing of coherent colour centres in diamond. *Nat. Photon.* 2017, 11, 77–80.
- [21] Chen, Y.-C.; Griffiths, B.; Weng, L.; Nicley, S.; Ishmael, S. N.; Lekhai, Y.; Johnson, S.; Stephen, C. J.; Green, B. L.; Morley, G. W.; Newton, M. E.; Booth, M. J.; Salter, P. S.; & Smith, J. M. Laser writing of individual atomic defects in a crystal with near-unity yield. *Arxiv:1807.04028* (2018).
- [22] Stephen, C. J.; Green, B. L.; Lekhai, Y. N. D.; Weng, L.; Hill, P.; Johnson, S.; Frangeskou, A. C.; Diggie, P. L.; Strain, M. J.; Gu, E.; Newton, M. E.; Smith, J. M.; Slater, P. S.; & Morley, G. W. Three-dimensional solid-state qubit arrays with long-lived spin coherence. *Arxiv:1807.03643* (2018).
- [23] Castelletto, S.; Almutairi, A. F. M.; Kumagai, K.; Katkus, T.; Hayasaki, Y.; Johnson, B. C.; & Juodkazis, S. Photoluminescence in Hexagonal silicon carbide by direct femtosecond laser writing. Accepted by *Opt. Lett.*
- [24] Nagy, R.; Widmann, M.; Niethammer, M.; Dasari, D. B. R.; Gerhardt, I.; Soykal, Ö. O.; Radulaski, M.; Ohshima, T.; Vučković, J.; Son, N. T.; Ivanov, I. G.; Economou, S. E.; Bonato, C.; Lee, S. Y.; & Wrachtrup, J. Quantum properties of dichroic silicon vacancy in silicon carbide. *Phys. Rev. Applied* 2018, 9, 034022.
- [25] Janzén, E., Gali, A., Carlsson, P., Gällström, A., Magnusson, B., & Son, N. T. The silicon vacancy in SiC. *Physica B: Condensed Matter.* (2009), 404(22), 4354-4358.
- [26] Fuchs, F.; Stender, B.; Trupke, M.; Simin, D.; Pflaum, J.; Dyakonov V.; & Astakhov, G.V. Engineering near-infrared single-photon emitters with optically active spins in ultrapure silicon carbide. *Nat. Commun.* 2015, 6, 7578.
- [27] Ohshima, T.; Satoh, T.; Kraus, H.; Astakhov, G. V.; Dyakonov, V.; & Baranov, P. G. Creation of silicon vacancy in silicon carbide by proton beam writing toward quantum sensing applications. *J. Phys. D Appl. Phys.* 2018, 51, 333002.
- [28] Magnusson, B.; Son, N. T.; Csóré, A.; Gällström, A.; Ohshima, T.; Gali, A.; & Ivanov, I. G. Excitation properties of the divacancy in 4H-SiC. *Phys. Rev. B.* 2018, 98, 195202.
- [29] Lagomarsino, S.; Sciortino, S.; Obreshkov, B.; Apostolova, Corsi, T. C.; Bellini, M.; Berdermann, E.; & Schmidt, C. J. Photoionization of monocrystalline CVD diamond irradiated with ultrashort intense laser pulse. *Phys. Rev. B.* 2016, 93, 085128.
- [30] Jones, S. C.; Braunlich, P.; Casper, R. T.; Shen, X.-A.; & Kelly, P. Recent progress on laser-induced modifications and intrinsic bulk damage of wide-gap optical materials. *Opt. Eng.* 1989, 28, 281039.
- [31] Steeds, J. W.; Evans, G. A.; Danks, L. R.; Furkert, S.; Voegeli, W.; Ismail, M. M.; & Carosella, F. Transmission electron microscope radiation damage of 4H and 6H SiC studied by photoluminescence spectroscopy. *Diam. Relat. Mater.* 2002, 11, 1923-1945.
- [32] Magyar, A. P.; Bracher, D.; Lee, J. C.; Aharonovich I.; & Hu, E. L. High quality SiC microdisk resonators fabricated from monolithic epilayer wafers. *Appl. Phys. Lett.* 2014, 104, 051109.

[33] Zargaleh, S. A.; Eble, B.; Hameau, S.; Cantin, J.-L.; Legrand, L.; Bernard, M.; Margaillan, F.; Lauret, J.-S.; Roch, J.-F.; von Bardeleben, H. J.; Rauls, E.; Gerstmann, U.; & Treussart, F. Evidence for near-infrared photoluminescence of nitrogen vacancy centers in 4H-SiC. Phys. Rev. B. 2016, 94, 060102.

Acknowledgements

The work was supported by grants from the Baden-Württemberg Stiftung Programm: Internationale Spitzenforschung, the ERC SMel and the BMBF BRAINQSENS.

Author contribution

Y.-C. C. carried out the PL, spectrum and HBT measurements with assistance from M. N., M. W., F. K., R. N., N. M. and C. B. and coordinated the work. P. S. S. conducted the laser writing. J. E. grew the SiC sample with supervision from P. B. Y.-C. C., J. W. and M. B. conceived and oversaw the project. All authors contributed to writing the manuscript.

Competing financial interests

The authors declare no competing financial interests.

Supporting information

Laser writing processing

The optical layout for the laser writing is shown in Figure S1. The laser processing was performed using a regeneratively amplified Ti:Sapphire laser (Spectra Physics Solstice) at a wavelength of 790 nm and a 1 kHz pulse repetition rate. The laser beam was expanded onto a liquid crystal phase-only spatial light modulator (SLM) (Hamamatsu X10468-02), which was imaged in a 4f configuration onto the back aperture of a 60× 1.4 NA Olympus PlanApo oil immersion objective. The SiC sample was mounted on precision translation stages (Aerotech x-y: ABL 10100; z: ANT95-3-V) providing three dimensional control. Prior to the objective the laser pulse was linearly polarised and had a duration which was measured to be 250 fs using an intensity autocorrelator (APE Pulsecheck). The pulse duration at focus will be slightly increased due to dispersion in the objective lens. To optimize the aberration correction, the phase pattern displayed on the SLM was adjusted to minimize the pulse energy needed to produce visible fluorescence at test processing positions of similar depth in the sample.

The point spread function of the processing laser is that of a focused Gaussian beam

$$I(r, z) = I_0 \cdot \frac{1}{1 + \left(\frac{z}{z_R}\right)^2} \cdot e^{-\frac{2r^2}{w_z^2}} \quad (S1)$$

where $w_z = w_0 \sqrt{1 + \left(\frac{z}{z_R}\right)^2}$ is the beam width at axial displacement z , w_0 is the beam waist and z_R is the Rayleigh range. Based on the numerical aperture of the objective lens, we estimate that $w_0 = 297$ nm and $z_R = 852$ nm.

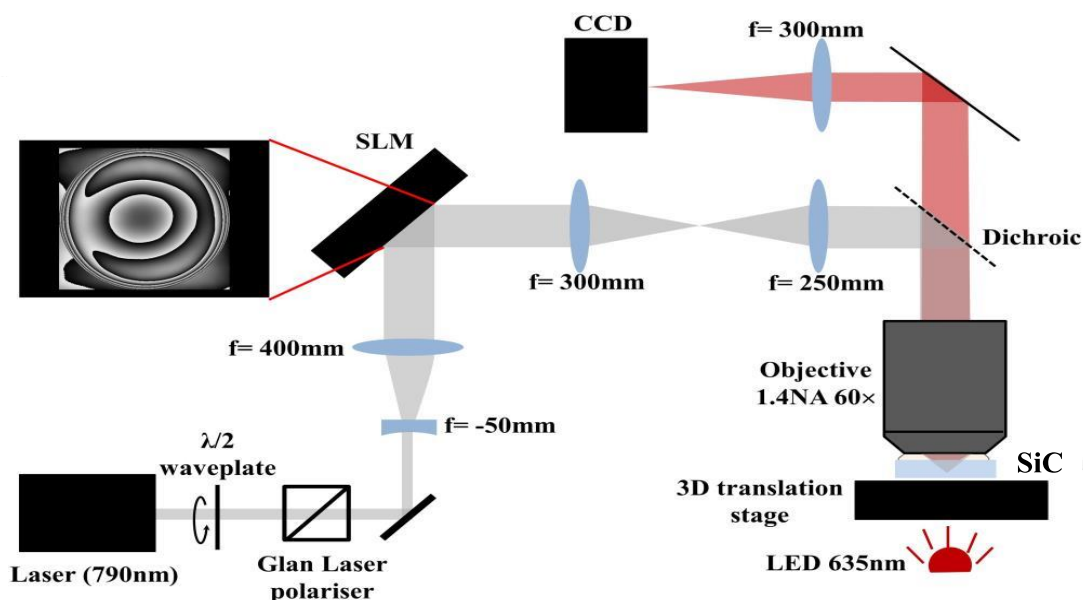


Figure S1. Aberration-corrected laser writing. (a) Schematic of laser processing apparatus. The phase pattern displayed on the SLM compensated optical aberration in the system and those introduced by focussing into the SiC sample.

Laser written array at depth of 40 μ m

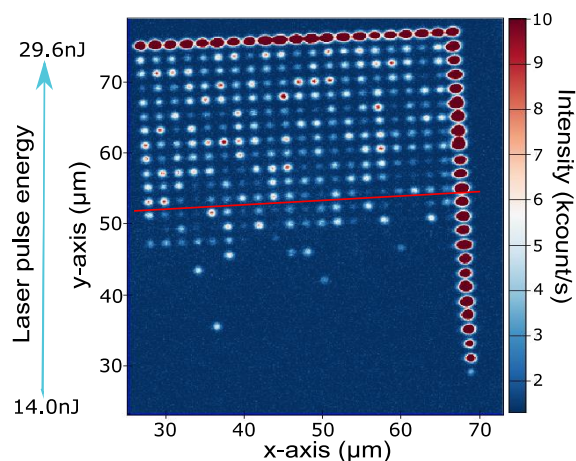


Figure S2. PL image of the Array B at a depth of 40 μm below the surface immediately after laser processing. The range of the laser pulse energy is provided on the left of the image. The red line at a pulse energy of 22.7 nJ indicates the pulse energy required to generate color centers in all 20 repeats.

Array B was generated with single laser pulses for each site in a 26×20 square grid with a pitch of 2 μm at a depth of 40 μm . Along one axis of the grids, the pulse energy, E_p , was varied from 29.6 nJ to 14.0 nJ to generate incremental degrees of damage to the lattice (see supporting information for detail). Along the other axis, 20 identical pulses were delivered to investigate statistics of the results for each pulse energy. The first column on the right-hand side of the array was created by 10 laser pulses of each energy, and the first row on the top of the array was created by 5 laser pulses with a laser pulse energy of 29.6 nJ. These features generated by multiple pulses serve as markers to locate the array. The heavy damage markers were also generated around Array A. Visible fluorescence was produced at every laser writing site when they had been exposed to pulses with $E_p \geq 22.7$ nJ (red line in Figure 2S).

Writing pulse energy

The laser pulse energy was precisely controlled using a rotatable half-waveplate before a Glan-Taylor polariser. 40 pulse energies used for the fabrication of Array A and Array B are shown in Table S1 and S2, respectively. The pulse energies were measured immediately before the objective. The pulse energies after the objective lens can be estimated by multiplying a factor of 0.7 due to the transmission loss of the objective lens, based on the manufacturer's specifications. For the pulse energy at the focus, one must also take into account Fresnel reflection at the SiC interface, which can be significant due to the large angles involved.

Laser pulse energy before objective (nJ)	Laser pulse energy after objective (nJ)
89.4	62.58
77.3	54.11
66.1	46.27
55.6	38.92
46.1	32.27
42.5	29.75
39.1	27.37
35.8	25.06
32.6	22.82
29.6	20.72
26.7	18.69
24.0	16.8
21.4	14.98
19.0	13.3
18.4	12.88
17.8	12.46
17.3	12.11
16.7	11.69
16.1	11.27
15.6	10.92
15.1	10.57
14.6	10.22
14.0	9.8
13.5	9.45
13.0	9.1
12.6	8.82
12.1	8.47
11.6	8.12
11.2	7.84
10.7	7.49
10.3	7.21
9.8	6.86
9.4	6.58
9.0	6.3
8.6	6.02
8.2	5.74
7.8	5.46
7.4	5.18
7.1	4.97
6.7	4.69

Table S1 Laser pulses energies used for the writing of defects in Array A.

Laser pulse energy before objective (nJ)	Laser pulse energy after objective (nJ)
29.6	20.72
28.9	20.23
28.1	19.67
27.4	19.18
26.7	18.69
26.0	18.2
25.4	17.78
24.7	17.29
24.0	16.8
23.3	16.31
22.7	15.89
22.1	15.47
21.4	14.98
20.8	14.56
20.2	14.14
19.6	13.72
19.0	13.3
18.4	12.88
17.8	12.46
17.3	12.11
16.7	11.69
16.1	11.27
15.6	10.92
15.1	10.57
14.6	10.22
14.0	9.8

Table S2 Laser pulses energies used for the writing of defects in Array B.

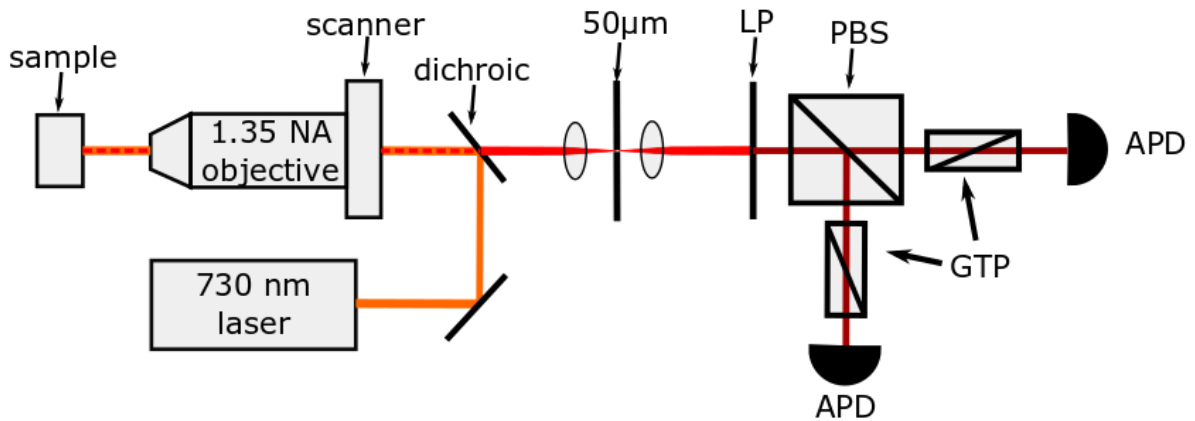


Figure S3. Experimental setup. Orange line represents the 730 nm excitation beam, the red line shows the fluorescence, dark red is the filtered fluorescence. LP indicates 850 nm long pass filter, PBS is polarizing beam-splitter, GTP is Glen-Taylor polarizer and APD is single photon Avalanche photon detector.

Optical characterization of the sample is carried out by a home-built confocal microscope depicted in Figure 2S. A red diode laser (Thorlabs HL7302MG, emission peak wavelength 730 nm, 40 mW) was focused via an oil objective (Olympus, UPLSAP 60 \times , NA 1.35) onto the sample to excite the silicon vacancies. The objective is mounted on a piezo-electric stage with a travel range in x-y-z of (100 \times 100 \times 10) μ m, respectively. Fluorescence from the emitters is collected by the same objective and passes through the dichroic mirror. Then, the fluorescence is focused into a 50 μ m pinhole to form confocal and spectrally filtered by an 850 nm long pass. The polarizing beam splitter (PBS), combined with two avalanche photon detectors, form a Hanbury-Brown and Twiss (HBT) setup. The addition Glen-Taylor calcite polarizers (GTP, Thorlabs GT10-B) are placed to suppress flash-back light from the APDs (Perkin Elmer SPCM-AQRH-15), which is caused by the avalanche of charge carriers accompanied by light emission.

Electron spins were manipulated by a radio-frequency electromagnetic field generated by a signal generator (ROHDE&SCHWARZ, SMIQ03B) and subsequently amplified by a broadband amplifier (Minicircuits ZHL-42W). RF irradiation was delivered to sample via a 20 μ m thick copper wire, which is placed close to the tested defects (typically \sim 30 μ m). For other details, see refs [1,2].

The low temperature measurements were conducted at a cryogenic temperature 4.2 K in a Montana Instruments Cryostation. The excitation was performed with a 785 nm diode laser. The fluorescence is filter by an 850 long pass filter and detected by a near infrared enhanced single photon avalanche photodiode (Excelitas, SPCM-AQRH-W5). PL spectra was recorded using a Czerny-Turner type spectrometer (Acton, SpectraPro300i, grating: 300 g mm^{-1}), combined with a back-illuminated CCD camera (Princeton Instruments, LN/CCD1340/400 EHRB/I).

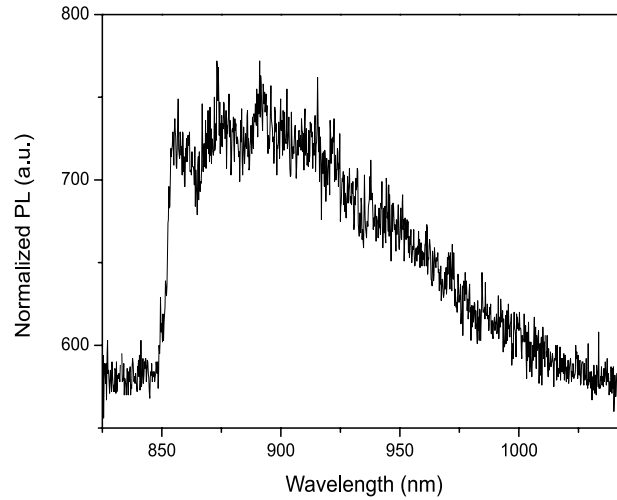


Figure S4. Typical spectrum of the marker generated by multiple laser pulses at 4.2 K.

Vacancy generation mechanism

Here, we discuss the mechanism of laser writing vacancies in dielectric materials. When a transparent dielectric material is illuminated by intense femtosecond laser, a large amount of excited electrons may be generated [3]. Relaxation channels of these free electrons in wide bandgap materials may produce intrinsic defects, resulting in photoinduced damages. For transparent materials, there is no linear absorption of the incident laser light to excite electrons due to the bandgap greater than photon energy. Therefore, a nonlinear mechanism must be responsible for the generation of free electrons creation [3, 4]. There two possible models have been proposed to describe the mechanism of free electron creation, which are tunnelling ionization (Zener breakdown) and multiple ionization (MPI). The details of these two model can be found in the ref. 3 and 4. The dominant mechanism for free electron generation is typically delineated by the Keldysh parameter [3]

$$\gamma = \frac{\omega}{e} \sqrt{\frac{mcn\epsilon_0 E_g}{I}}$$

where ω and I are the laser frequency and intensity, while m , c , n , ϵ_0 and E_g are the electron effective mass, speed of light in vacuum, linear refractive index, permittivity of free space and the direct bandgap respectively. MPI is dominant over tunnelling breakdown for $\gamma > 1$ corresponding to

$$I < \frac{mcn\epsilon_0 E_g \omega^2}{e^2}.$$

For the parameters used here ($m = 0.42m_e$ [5], $n = 2.59$, $E_g = 3.23 \text{ eV}$ and $\omega = 2.4 \times 10^{15} \text{ s}^{-1}$) assuming a pulse duration of 300 fs and a beam waist of 350 nm, the equation above predicts that MPI will dominate for pulse energies below about 12.27 nJ.

Reference

- [1] Balasubramanian, G. *et al.* Ultralong spin coherence time in isotopically engineered diamond. *Nat Mater* **8**, 383–387 (2009).
- [2] Zhao, N. *et al.* Sensing single remote nuclear spins. *Nat Nano* **7**, 657–662 (2012).

- [3] Mao S.S. et al. Dynamics of femtosecond laser interactions with dielectrics. *Appl. Phys. A.* 79, 1695-1709, (2004).
- [4] Schaffer C. B. et al. Laser-induced breakdown and damage in bulk transparent materials induced by tightly focused femtosecond laser pulses. *Meas. Sci. Technol.* 12, 1784, (2001).
- [5] Son N. T. et al. Electron effective masses in 4H SiC. *Appl. Phys. Lett.* 66, 27, (1995).